IEEE Access
Multidisciplinary | Rapid Review | Open Access Journal

Received December 28, 2019, accepted January 2, 2020, date of publication January 13, 2020, date of current version January 22, 2020.

Digital Object Identifier 10.1109/ACCESS.2020.2965982

Electrical Impedance Myography Applied to Monitoring of Muscle Fatigue During Dynamic Contractions

L. K. HUANG[1,2], L. N. HUANG[1,2], Y. M. GAO[1,2], Ž. LUČEV VASIĆ[3], M. CIFREK[3], AND M. DU[1,4]

[1]College of Physics and Information Engineering, Fuzhou University, Fuzhou 350116, China
[2]Key Laboratory of Medical Instrumentation & Pharmaceutical Technology of Fujian Province, Fuzhou 350116, China
[3]Faculty of Electrical Engineering and Computing, University of Zagreb, 10000 Zagreb, Croatia
[4]Key Laboratory of Eco-Industrial Green Technology of Fujian Province, Wuyi University, Nanping 354300, China

Corresponding author: Y. M. Gao (fzugym@gmail.com)

This work was supported in part by the National Natural Science Foundation of China U1505251, in part by the Project of Chinese Ministry of Science and Technology 2016YFE0122700, an in part by the Project of S&T Department of Fujian Province 2018I0011.

ABSTRACT Muscle fatigue, as a common physiological phenomenon, has attracted much attention in the fields of rehabilitation and athletic training. A wearable technology for monitoring the muscle fatigue anytime and anywhere is urgently needed. In this paper we apply Electrical impedance myography (EIM) technique, usually used for non-invasive detection of neuromuscular diseases with the four-electrode array, for evaluation of the local muscle fatigue status via the variation of electrical impedance. An equivalent multilayer inhomogeneous 3D finite element model of human arm was built in order to optimize the four-electrode configuration to improve EIM detection sensitivity. Current density in muscle layer and differential potential of induction electrodes were selected as the evaluation indexes for optimization. Then the *in vivo* experiments of dynamic contraction with different maximal voluntary contractions (MVC) were performed on the *biceps brachii* muscle of eight healthy volunteers. The results showed that muscle resistance (R) decreased almost 8 Ω from the completely relaxed muscle to exhaustion, which is the same trend as for the median frequency (MF) of measured surface electromyography (sEMG) signals. The model and experiments in this paper indicate the feasibility and efficiency of EIM for detection of muscle fatigue using wearable devices.

INDEX TERMS Electrical impedance myography, muscle fatigue, optimized electrode configurations, finite element method, surface electromyography.

I. INTRODUCTION

The continuous movement of muscles gradually reduces their work capacity, maximum contraction force and output power [1]. This physiological phenomenon is known as a muscle fatigue and is closely related to changes in muscle microstructure [2]. If muscle fatigue is not properly handled, it can cause muscle strain and seriously affect the daily lives of people or, especially, the physical exercise of athletes. However, most of the existing muscle fatigue detections are conducted in hospitals or rehabilitation centers and the patients cannot detect muscle fatigue anytime and anywhere or perform self-measurement at home. A wearable device that can monitor muscle fatigue at any time would be very useful for exercise rehabilitation, muscle disease diagnosis, sports training, and other fields.

Several indicators, such as muscle oxygen saturation [3], lactic acid concentration [4], ultrasound image entropy [5], and surface electromyography (sEMG) [6], [7], are used for muscle fatigue evaluation. Among these indicators, sEMG is the most common and widely used [8]–[10]. The amplitude and spectrum characteristics of sEMG, which has the advantages of non-invasiveness and simple operation, can directly reflect the progressive process of fatigue [11], [12]. However, sEMG has small amplitude (order of microvolts), wide frequency variation range, and is prone to interference

The associate editor coordinating the review of this manuscript and approving it for publication was Larbi Boubchir.

from other physiological signals and electromagnetic noise. Furthermore, the acquisition circuit and digital signal processing are complicated, thereby making sEMG integration into wearable devices difficult.

Electrical impedance myography (EIM) is a new non-invasive bioelectrical impedance technique based on the four-electrode array [13]. This technique evaluates the health status of a local muscle by applying a high-frequency, low-intensity alternating current to the muscle of interest. EIM can also be used in clinical diagnosis and efficacy evaluation of various neuromuscular diseases [14]. During muscle fatigue, the lactic acid content of muscle cells in muscle fibers increases, thus slowing down the conduction speed of electrical signals in muscle fibers [15]. The EIM method detects changes in impedance due to muscle abnormalities or muscle fatigue, and can ultimately provide an assessment of muscle fatigue. Compared to the traditional sEMG approach for muscle fatigue assessment, the detection parameters (R, reactance, phase) of EIM signals have many advantages: large EIM signal amplitude, controllable frequency, and simple pretreatment procedure. Therefore, EIM could be used as a new, low complexity and high feasibility method of real-time muscle fatigue monitoring, which can easily be integrated with various wearable devices.

In early EIM studies this technique was mainly involved in the clinical diagnosis of neuromuscular diseases and the preliminary evaluation of non-neuromuscular diseases. Wang *et al.* [16] studied neuromuscular diseases in the legs of mice via finite element modeling. Li *et al.* [17] researched the difference of EIM parameters between patients with spinal cord injury and normal patients. Jafarpoor *et al.* [18] investigated the effects of muscle size and subcutaneous fatness on EIM parameters. In addition, Orth and Le *et al.* conducted relevant research on the EIM parameters after muscle fatigue [19], [20], which explained a relation between the EIM parameters of *biceps brachii* muscle and the degree of muscle fatigue in static contraction mode. The aforementioned research findings contribute to the possibility of using EIM for muscle fatigue evaluation. The existing research of *biceps brachii* muscle fatigue indicates the following three shortcomings:

1) The present results show that the optimization on electrode configuration could improve EIM detection efficiency. However, the present studies are less concerned with electrode configuration and lack in corresponding model analysis and evaluation.
2) Only the static contraction process was explored, and the change of EIM parameters in dynamic contraction mode was not studied.
3) Only the EIM method was used to evaluate muscle fatigue, and no comparison was made with other recognized methods.

This paper aims to conduct model and experimental research on muscle fatigue by using the EIM method due to its easy integration into wearable devices. By establishing a three-dimensional (3D) model of the entire arm, the optimal electrode configuration was obtained using a finite element simulation. The variation in EIM parameters under dynamic contraction were investigated and compared with sEMG measurements to verify the feasibility and rationality of using EIM parameters as a muscle fatigue evaluation index. The results of this study provide technical support and theoretical guidance for the development of wearable equipment for the evaluation of the degree of muscle fatigue. The rest of this paper is organized as follows. In Section II a 3D arm simulation model for optimization of EIM electrode configuration is described, together with measurement setups for *in vivo* EIM and sEMG dynamic contraction measurements. The results are presented in Section III. Optimal EIM electrode configuration was calculated and used in the EIM and sEMG measurements of muscle fatigue. Two evaluation parameters (proposed EIM parameter R and standardly used median frequency of sEMG signals) obtained in the *in vivo* experiments were compared. Finally, Section IV presents the conclusion of this study.

II. METHODS

A. ESTABLISHMENT OF ARM SIMULATION MODEL

Structure of the volunteers' arm is shown in Fig. 1 (a) which from the website (https://www.medical-artist.com/anatomy-images/illustrations-of-muscles/). From the perspective of human anatomy [21], [22], the complex structure of the human body is reasonably simplified and a 3D arm model consisting of four layers (bone, muscle, fat, and skin) is constructed. The developed geometric model is shown in Fig. 1(b). The upper and lower arms are modeled as two elliptical cylinders joined seamlessly in the elbow joint, right part being the upper and left part being the lower arm. The long half-axis a_n and the short half-axis b_n ($n = 1, 2, 3$) at three cross-sections (wrist, elbow, and shoulder) are marked in the Fig. 1, together with the measurement principle and the positions of EIM electrodes. here x and y represent the spacing between the successive electrodes and section α represents the cross-section at the midpoint between the induction electrodes.

In order to get the geometric model parameters, physiological parameters of eight volunteers were measured: BMI, fat rate, muscle rate, bone mass were measured using the PICOOC Latin Smart Body Scale (PICOOC Inc., Beijing, China) and circumferences of the volunteer's arm were measured manually. Results are presented in Table 1 [23]. Experiment numbers 1–4 were female volunteers and 5–8 were male volunteers. Parameters BL, LAC, EC, and UAC in Table 1 stand for brachium length, lower arm (wrist) circumference, joint circumference (elbow), and upper arm (shoulder) circumference, respectively. Brachium length (BL) was measured as a distance between the wrist and the armpit of the volunteers. Using the average (AVG) and standard deviation (SD) of physiological parameters of eight volunteers in Table 1, the long and short semi-axis of each tissue layer was calculated based on the arm circumference in

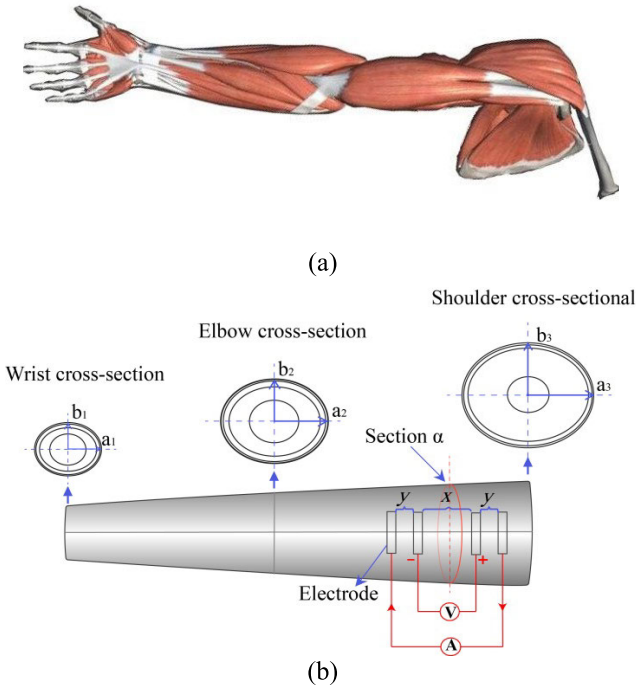

FIGURE 1. (a) Illustration of the real human arm. (b) Human body 3D arm model has four layers (bone, muscle, fat, and skin), and section α represents the cross-section at the midpoint between the induction electrodes.

TABLE 1. Physiological parameters of eight volunteers.

	BMI	Fat (%)	Muscle (%)	Bone (kg)	BL (cm)	LAC (cm)	EC (cm)	UAC (cm)
1	17.01	14.00	80.50	2.10	45.00	15.00	20.50	22.00
2	19.65	23.40	72.50	2.10	46.00	15.00	20.00	23.00
3	16.60	20.90	74.60	2.00	48.00	14.00	20.50	21.50
4	21.40	29.00	66.90	2.20	45.00	16.00	21.00	25.00
5	21.20	17.20	78.60	2.50	46.00	16.00	24.50	26.00
6	21.40	15.10	80.50	2.80	48.00	17.00	24.50	26.50
7	27.90	25.60	70.70	3.20	46.00	18.00	24.50	28.00
8	17.70	13.30	82.10	2.20	45.00	15.50	21.00	22.00
AVG	20.36	19.81	75.8	2.39	46.13	15.81	22.06	24.25
SD	3.40	0.05	0.05	0.39	1.17	1.17	1.91	2.29

joints and the proportion of bone, muscle, and fat. In addition, anatomical data show that the average thickness of human skin is 1∼2 mm [24], so the thickness of skin layer is defined as 1.5 mm in this paper. Calculated equivalent geometric parameters of each layer are shown in Table 2 [23].

When measuring EIM parameters of *biceps brachii* muscle, the human body acts as an electric medium; therefore, the electrical conductivity σ and relative permittivity ε_r of each layer of the human body should be defined in the simulation model. In a muscle tissue, after depolarization induced by an external excitation source, the electric current will propagate in all directions, but the propagation speed will vary based on the muscle fiber orientation. Therefore, the conductivity and relative permittivity of the muscle tissue are set to be anisotropic. The muscle electrical properties were obtained from the measurements of electrical conductivity and relative permittivity of gastrocnemius muscle in mice at

TABLE 2. Equivalent geometric tissue parameters at three cross-sections of the human arm.

Tissue layer	Wrist		Elbow joint		Shoulder	
	a_1 (cm)	b_1 (cm)	a_2 (cm)	b_2 (cm)	a_3 (cm)	b_3 (cm)
Bone	0.59	0.56	1.22	0.93	0.63	0.60
Muscle	2.15	1.61	3.21	2.14	3.49	2.61
Fat	2.74	2.04	4.07	2.70	4.45	3.32
Skin	2.89	2.19	4.22	2.85	4.60	3.47

Harvard Medical College [16]. The skin, fat, and bone are set to be isotropic, and the parameters are derived from the Gabriel model [25].

B. ELECTROMAGNETIC MODELING OF EIM ELECTRODES CONFIGURATION

Results of EIM measurement depend on the EIM electrodes configuration on the skin. In this section, the AC/DC module in COMSOL Multiphysics 5.2a simulation software is used to find the optimal configuration of EIM electrodes in EIM method by using finite element method. Discussions are made on the ways to optimize distance between the EIM electrodes and use minimal excitation signal for maximal measured potential difference. This optimal configuration provides good precondition for the front-end signal detection system of a wearable device.

The governing equations of the EIM finite element method are based on the Maxwell's equations because they can describe the nature of the electromagnetic field acting on organisms. In the frequency range from 1 kHz to 1 MHz, the human body acts as the transmission medium for coupling and propagation of exciting current signals, which meet the quasi-electrostatic field conditions [26]. Therefore, we use the simplified Maxwell's equation, as shown in Eq. (1), [27]:

$$\nabla [\lambda \nabla V] = 0, \tag{1}$$

where $\lambda = \sigma + j\omega\varepsilon$ is the complex conductivity of biological tissue, and V is the applied voltage.

When the signal is injected to the electrode on the model surface, the voltage is constant V_{in} as shown in Eq. (2), according to the Dirichlet boundary conditions [28]:

$$V = V_{in}. \tag{2}$$

The conditions of current and voltage continuity must be satisfied at boundaries between all adjacent layers, as well as at the boundary between the skin layer and electrodes, as shown in Eq. (3):

$$\begin{cases} V_i = V_{i-1} \\ J_i = J_{i-1} \end{cases} \quad (i = 2, 3, 4), \tag{3}$$

where V_{i-1} and V_i are voltages in adjacent layers, J_{i-1} and J_i are current densities in adjacent layers, the subscript i represents tissue layers, and values are 2, 3, and 4, respectively.

The following steps are necessary when evaluating the potential difference and current density at EIM induction electrodes: set up a suspension potential in AC/DC module, input 1 mA current signal to the arm model, set up a boundary probe to detect the potential between the two inner EIM electrodes, and calculate voltage V_{sense}. Moreover, two integral functions of current density are defined, and the integral domain is set for calculating overall current density generated at the induction (outer) electrodes and applied to the arm, J_{arm}, as well as for calculating current density in muscle tissue, J_{muscle}. In many early studies, the 50 kHz signal frequency was sufficiently sensitive for neuromuscular diseases detection [29], [30]; therefore, in this paper we will also focus on the 50 kHz EIM signals.

From the perspective of a wearable device, higher potential difference between the induction electrodes leads to a higher voltage detection at the receiving end. In addition, if the signals injected into the human body can flow through the muscle layer, then the measured EIM parameters can accurately reflect the muscle characteristics and the requirements and objectives of this research can be achieved. Therefore, in this paper electrode configuration will be optimized based on two parameters, which should be as high as possible: 1) the ratio of current density in the muscle layer and the current density in the whole arm (J_{muscle}/J_{arm}) and 2) the potential difference achieved at the voltage electrodes (V_{sense}). The optimal electrode distance was obtained by measuring the length of the *biceps brachii* of each volunteer and according to the finite element modeling analysis. According to the simulation platform in Fig. 1, the electrodes attached to the skin surface in our model are obtained by Boolean operation. References [31], [32] show that the distance between the electrodes is mainly set in three ratios of y: x: y in Fig. 1(b) 1:1:1, 1:2:1, and 1:3:1, according to the size of the *biceps brachii* muscles of healthy adults. The distance between the two internal EIM electrodes was set to $x = 24$ mm, as shown in Fig. 1. The distance between the external and internal electrodes (y in Fig. 1) is different and is set to 8 mm, 12 mm, and 20 mm. Although according to the ratio of 1:1:1, y should be set to 24 mm, the maximum value of y was set to 20 mm because of the limited length of a volunteer's *biceps brachii* muscles.

C. EIM AND EMG IN VIVO MEASUREMENTS

This study was approved by the First Affiliated Hospital of Fujian Medical University and the Fujian Provincial Key Laboratory of Medical Devices and Medical Technology. Informed consent was obtained from the volunteers prior to the measurements.

For obtaining the optimal electrode configuration the following two evaluation indicators were used: 1) ratio of current density in the muscle layer and current density in the arm (J_{muscle}/J_{arm}) and 2) potential difference between the voltage electrodes (V_{sense}). This configuration will also be applied in the following *in vivo* experiments to establish a foundation for the measurements accuracy testing.

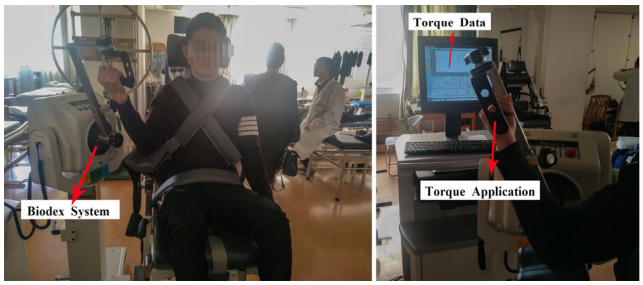

FIGURE 2. Diagram of MVC measurement: (a) Front view, (b) Side view.

TABLE 3. MVC data of eight volunteers.

Number	1	2	3	4	5	6	7	8
MVC (N•m)	28.7	30.2	36.4	29.1	57.0	48.8	64.5	62.0

Before the in vivo experiment, the maximal voluntary contraction (MVC) of each volunteer was tested. In the experiment, different contraction strengths (such as 20% MVC, 40% MVC, 60% MVC) are used to indicate different contraction states of muscles. The MVC of eight healthy volunteers was measured using the Biodex System 4 multi-joint muscle strength assessment training system (minimum passive movement speed: 0.25 degrees/s, minimum passive motion torque: 0.5 ft-lb (0.68 Nm), minimal isotonic motion torque: 0.5 ft-lb (0.68 Nm)) developed by the U.S. BIODEX Company. The test process is shown in Fig. 2. Volunteers sit on matching seats that can be adjusted in height and direction and their upper body posture is kept still by the adjustable restraints. The volunteers had to hold the torque device obtaining the 90° elbow joint that aligned with the center of the power shaft and to perform the maximal isometric contraction. Three measurements of MVC for each volunteer were taken in total, with a one minute break after each measurement. Finally, the average of the three measurements was calculated and used as the MVC of the right arm. The MVC values for each participant are shown in Table 3.

The MVC data of volunteers in Table 3 were further used in a dynamic muscle contraction experiment (lower arm flexion) shown in Fig. 3, for which the experimental investigation of muscle electrical impedance changes was carried out. In many studies, resistance R is the first parameter to change during muscle contraction [19], [20] while reluctance and phase experience minimal changes. Therefore, this paper mainly discusses R parameters of *in vivo* experiments.

A block diagram and photography of a lower arm flexion experiment are shown in Figs. 3 and 4, respectively. EIM measurement setup consists of a signal generator (Rigol DG4162), constant current source, four electrodes placed on *biceps brachii* muscle, Agilent 1141A differential probe, and Agilent MSO7054A oscilloscope.

In the experiment, the AC voltage signal with a frequency range from 1 kHz to 1 MHz and 1 V amplitude is generated and fed to the constant current source. The constant

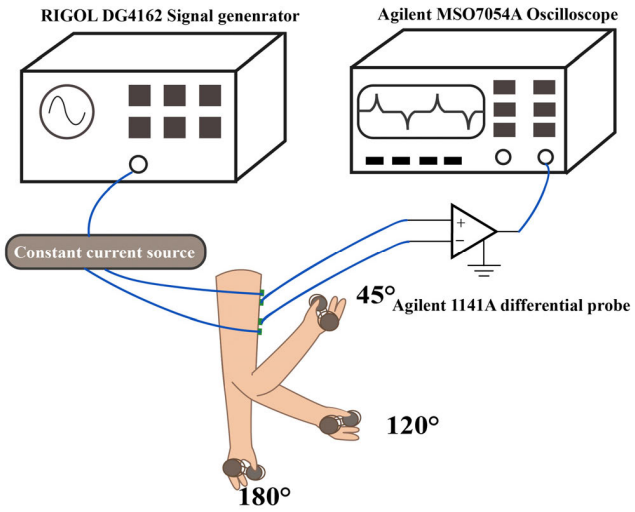

FIGURE 3. Block diagram of a lower arm flexion experiment.

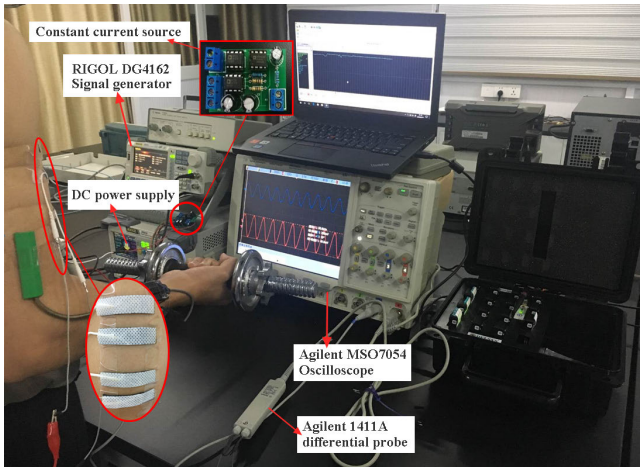

FIGURE 4. EIM human experiment scene.

current source is built around a current feedback amplifier AD844 and operational amplifier OP27 and is used to convert AC voltage signal into constant 1 mA current signals. The current signal is then loaded into the *biceps brachii* muscle by four side-by-side electrodes of the same size. When placing the electrodes, a position of the volunteer's *biceps brachii* muscle belly was determined and used as a reference, The four electrodes were placed symmetrically along the direction of the arm with the *biceps brachii* muscle belly as the center. The configuration of the electrodes was obtained by electromagnetic modeling. According to results in Table 5, physiotherapy electrodes made by Shanghai Litu Medical Equipment Co., Ltd were selected as *in vivo* experimental electrodes. Their conductivity and relative permittivity are 5.0×10^5 S/m and 1.0 [33], respectively, and their size is 40 mm × 10 mm. The coupling voltage signal measured between the voltage electrodes at the receiving end is displayed by the oscilloscope in real-time to obtain the impedance parameters. The Agilent 1141A differential probe was used for connecting the electrodes on the body and the oscilloscope in order to solve the common-ground problem between the receiving and the transmitting electrodes [25], [26].

TABLE 4. J_{muscle}/J_{arm} and V_{sense} with different electrode spacings at 50 kHz.

	y = 8 mm	y = 12 mm	y = 20 mm
J_{muscle}/J_{arm}	90.14%	90.58%	91.06%
V_{sense}	0.064	0.055	0.042

Volunteers were asked to perform repeated lower arm flexions until exhaustion while holding a dumbbell with weights of of 20%, 40%, and 60% of their MVC. One dynamic contraction cycle starts with the arm naturally drooping at 180° elbow angle. During one contraction cycle the elbow angle decreases from 180° to 45° and then increases back to 180°, as in Fig. 3. EIM parameters were sampled during this muscle fatigue process at the half-cycle point (45°), every 10 cycles.

At the same time, eight healthy volunteers also participated in the measurements of surface EMG signals during dynamic contractions. EMG signals were acquired in real-time using the Trigno Lab wireless surface EMG acquisition system produced by the Delsys Company, USA. In the experiment, the EMG wireless sensor was adhered to the skin using Delsys adhesive to ensure full contact between the sensor and the skin. EMG sensor was placed on the center of the muscle belly away from the tendon and muscle edge, along the longitudinal muscle fibers and the sampling frequency of the EMG was set to 1 kHz. Measured sEMG signals were used for verification of EIM muscle fatigue estimation.

III. RESULTS

A. ELECTRODE CONFIGURATION SIMULATION RESULTS

Results of simulations described in II. METHODS. B are presented in Table 4. In all three cases, the electrode can effectively inject the current into the muscle layer, which conforms to the research content of muscle fatigue. It is shown that at the 50 kHz frequency, current flowing through the muscle layer accounts for more than 90% of the overall current in the arm. The value of J_{muscle}/J_{arm} increases with the space between exciting electrodes, while the modulus of voltage V_{sense} decreases. The difference between the shortest (8 mm) and longest (20 mm) distances is less than 1 %, and the modulus of V_{sense} parameter is the largest for $y = 8$ mm.

The current density at α cross-section, in the middle between the electrodes, is shown in Fig. 5. It can be seen from the current density distribution diagram in Fig. 5 that when $y = 8$ mm, the current density of the muscle layer is the largest.

In overall, the optimal electrode spacing setting for the excitation electrode is $y = 8$ mm. The larger the potential difference, the greater the current density in the muscle layer, which is conducive to the detection of the sensing electrode of the wearable device.

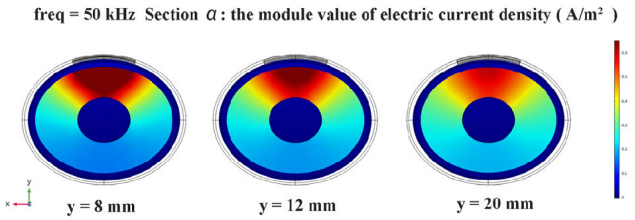

FIGURE 5. Central cross-sectional current density distribution for three different electrode spacings at 50 kHz.

TABLE 5. J_{muscle}/J_{arm} and V_{sense} with different electrode materials at 50 kHz.

	Aluminum electrode	Silver electrode	Physiotherapy electrodes
J_{muscle}/J_{arm}	88.01%	89.27%	90.14%
V_{sense}	0.059	0.061	0.064

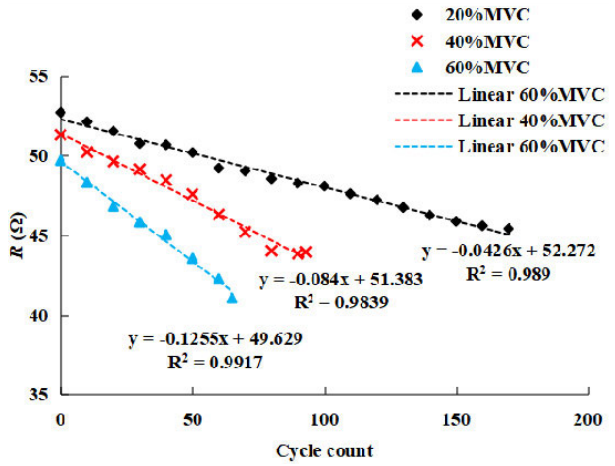

FIGURE 6. Dynamic contraction experiments of muscles under different weight-bearing conditions (20%, 40%, and 60% MVC). The down trend of *R* (50 kHz) in the muscles of Volunteer 1 from complete relaxation to extreme fatigue.

On the premise of the above experimental results, in order to study the effect of different electrode materials on the experiment, three more common electrode materials (aluminum electrode, silver electrode, physiotherapy electrode) [33] were selected as the research objects. The experimental results obtained through simulation under the same conditions are shown in Table 5. As can be seen from Table 5, the J_{muscle}/J_{arm} and V_{sense} parameters of the physiotherapy electrode is the largest, so the physiotherapy electrode is selected as the electrode for subsequent *in vivo* experiments.

B. EXPERIMENTAL RESULTS OF EIM APPLIED TO MUSCLE FATIGUE

Fig. 6 shows the relationship between *R* parameters and contraction time of *biceps brachii* muscle under different loads (20%, 40%, and 60% MVC) at 50 kHz measured on the volunteer 1. The muscle *R* data at different load levels show a linear decreasing trend with the increase in contraction time.

TABLE 6. Average value of three parameters (without fatigue *R*, exhaustion *R*, drop-out value *R*) in muscle dynamic contraction experiments of 8 volunteers under the different load levels.

	Without fatigue *R* (Ω)	Exhaustion *R* (Ω)	Drop-out value *R* (Ω)
20%MVC	53.92	46.00	7.92
40%MVC	52.09	44.16	7.93
60%MVC	50.22	42.10	8.12
Average	–	–	7.99

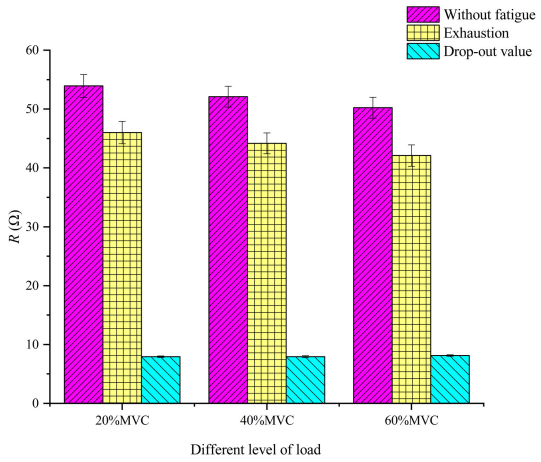

FIGURE 7. The average *R* and drop-out standard deviation value of eight volunteers in dynamic contraction experiments (volunteer's *biceps* from without fatigue to exhaustion) under the different load levels.

Moreover, it is evident that the slope of the linear fit line is different for different loads.

Using the experimental platform in Fig. 4 for dynamic contraction experiments under different load levels, the average resistance and drop-out values of 8 volunteers before and after fatigue were obtained, and the results are presented in Table 6. The average *R* and drop-out standard deviation of eight volunteers was calculated before and after muscle fatigue experiment (under different load levels), and the results are shown in Fig. 7.

The *R* values of 8 volunteers before (without fatigue) and after fatigue (exhaustion) were significantly different ($p < 0.01$). It can be seen from Table 6 that the drop value of *R* of eight volunteers during the dynamic muscle contraction experiment was about 8 Ω. It can be obtained from Fig. 7 that the standard deviation of the eight volunteers is about 1.9 Ω.

C. EXPERIMENTAL RESULTS OF SEMG APPLIED TO MUSCLE FATIGUE

Classical frequency-domain index for evaluating muscle fatigue from measured EMG signals, often used as reference value, is a median frequency (MF) [34]. Using the experimental method described in Section II.C, the EMG signals were measured for different loads in dynamic contraction scenes and then processed in MATLAB. The obtained MF

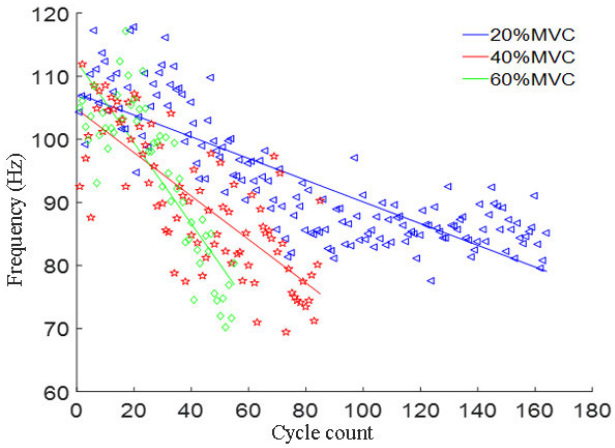

FIGURE 8. MF and linear fitting curves of volunteer 1 in the muscle dynamic contraction experiment for different load levels.

and linear fitting curves under loads of 20%, 40%, and 60% MVC, respectively, are shown in Fig. 8. Fig. 8 shows that higher muscle load level will result in more rapid decline of MF and will speed up the muscle fatigue process.

By comparing Fig. 6 and Fig. 8, it is found that both the frequency domain index (MF) of sEMG and the EIM parameter index (R) show a downward trend. In the dynamic contraction experiment, these two parameter values continue to decrease as the fatigue level increases. Therefore, in this paper the frequency domain index (MF) of sEMG is used as the comparison index. A comparative analysis of the two parameters will be conducted in the next section to ensure the rationality and feasibility of the EIM parameter (R) for muscle fatigue evaluation.

D. COMPARATIVE ANALYSIS OF EIM AND SEMG MUSCLE FATIGUE PARAMETERS

EIM and sEMG signals were acquired simultaneously during dynamic contractions until the exhaustion. Achieved number of contractions cycles decreased with an increasing load. The experimental data are shown in Fig 9 for (a) 20% MVC, (b) 40% MVC, and (c) 60% MVC load and include both muscle fatigue index (MF) calculated from sEMG signals (blue) and measured R measured using EIM electrodes (red). In order to facilitate comparison of changes in R parameters and the MF at different load levels, the number of cycles obtained in Fig. 6 and Fig. 8 is normalized.

Fig. 9 shows that the absolute values of the linear fit slope are higher for the heavier load, that is, the decline speed is fast. In addition, the linear fit equation of the MF and R parameters shows that the decline slope of R linear fit line for each load is nearly 2/5 that of the MF. Thus, the decrease rate of the R is not as fast as the decrease of MF, but a considerable consistency is observed in the decline regularity of the two curves. Therefore, EIM is feasible for muscle fatigue evaluation, and the rationality of this approach was verified.

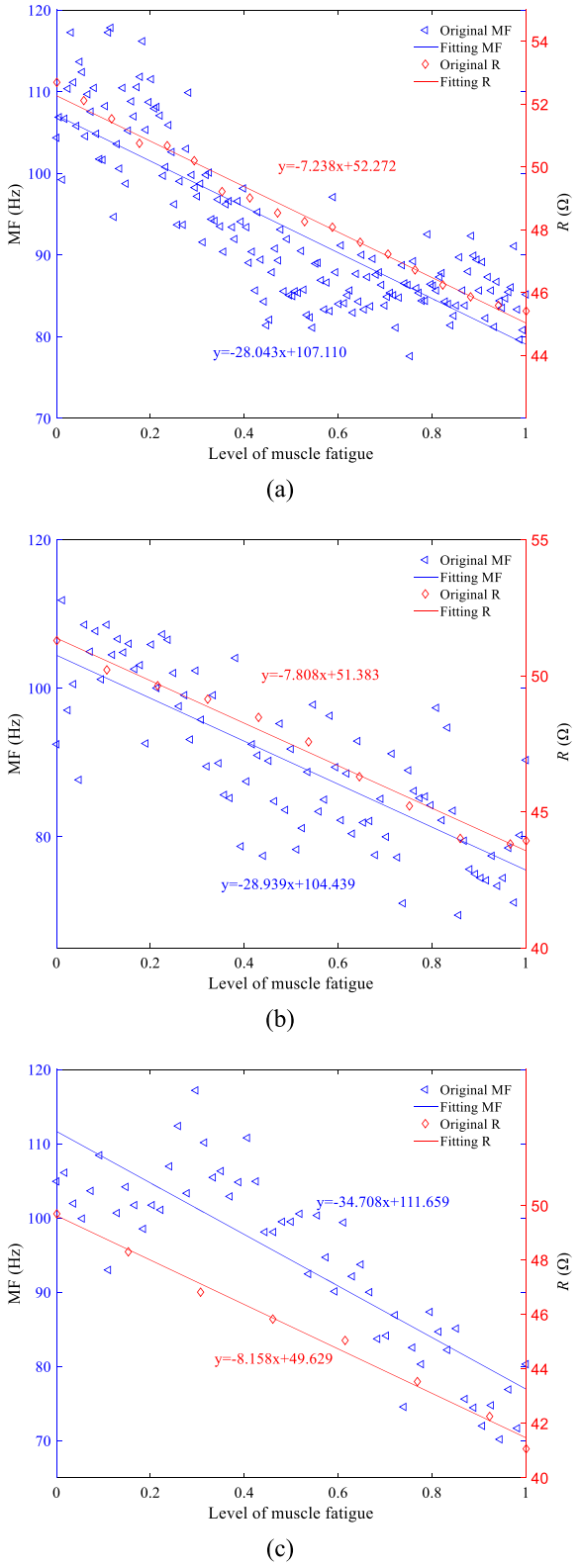

FIGURE 9. Curve trend chart of MF and R under different loads during dynamic contractions for: (a) 20% MVC, (b) 40% MVC, (c) 60% MVC.

IV. DISCUSSION

It can be seen from Table 4 that when the electrode distance is larger, the J_{muscle}/J_{arm} value will be large. The reason for

this phenomenon may be that the J_{muscle}/J_{arm} is determined by the size of the muscle layer and its conductive properties. When the injected constant current signal flows through the arm model, the larger the electrode spacing, the proportion of circuit density occupied by the muscle layer is greater, which is consistent with the results in [35], [36]. The current density value in the middle cross-section reaches the maximum when $y = 8$ mm. This finding is due to the small distance between excitation electrodes, which results in the closeness of the middle cross-section to the excitation electrode and consequently in a high current density. The modulus of V_{sense} decreases with the increase in the distance between exciting electrodes. The cause may be that a large distance between the electrodes results in an additional electrical signal loss on the human body. Therefore, a potential difference detected on the induction electrode leads to a small modulus of V_{sense}.

The MVC of each volunteer is different. In the subsequent experiments, the corresponding weight of the dumbbell is set according to the MVC of different volunteers. Different load levels make volunteers' EIM parameters (R) change with different trends. In Figure 6, it can be seen that under different load levels (20% MVC, 40% MVC, 60% MVC), the R parameters decreases with increasing fatigue level, and the heavier the muscle load, the faster the decline. The difference in the slope of the R value under different weights is relatively large, which may mean that the muscle R parameters could be used for the recognition of the fatigue state caused by different loads in a given period. At the same time, it can be found that there are obvious differences of the R under different load levels. The reason may be that the muscles undergo many physiological and morphological changes from the resting state to the contracted state after they begin to contract. During exercise, an increase in muscle blood flow enlarges the cell membrane volume [37], thereby reducing the number of cell walls. At the same time, the cell wall will resist along the direction of muscle fibers, and when the muscle is under load, it will produce an opposite contraction to maintain its original strength level. The greater the force exerted on the muscles under the same conditions, the higher the amount of heat required, so it will stimulate more blood flow and activate more muscle fibers, resulting in increased muscle conductivity and decreased R.

Baidya and Ahad in [38] used the genetic algorithm and the finite element model of EIM to optimize the electrode configuration of EIM. Their optimal electrode configuration is: the optimal electrode spacing between the excitation electrodes is 33 mm, the optimal electrode spacing between the induction electrodes is 7 mm, and the surface area of the electrodes is 7 mm $\times$ 7 mm. However, their optimized electrode configuration may not be suitable for *in vivo* experiments on the biceps because of its limited muscle length. The optimal electrode configuration obtained by finite element analysis in this paper is: the optimal electrode spacing between the excitation electrodes is 8 mm, the optimal electrode spacing between the induction electrodes is 24 mm, and the surface area of the electrodes is 40 mm $\times$ 10 mm. The optimized electrode configuration was applied to volunteers' biceps for *in vivo* experiments.

V. CONCLUSION

EIM is a novel and non-invasive electrical impedance technology, which can monitor the characteristics of bioelectrical signals for long-term and use them for continuous evaluation of the muscle function status. In the muscle dynamic contraction fatigue experiment, the subjects are considered to reach the semi-fatigue point when the measured R parameters decrease by approximately 4 Ω. With the further R decrease approaching 8 Ω, the muscle fatigue is considered to reach its limit. Thus, the subjects can adjust their exercise intensity according to the magnitude of R decline to avoid muscle fatigue or the damage caused by excessive exercise.

In this paper, the finite element analysis method is used to simulate the bone weight, muscle size, fat thickness, electrode spacing and electrode shape of the individual arm to obtain the optimal electrode configuration method and improve the detection efficiency of EIM. In addition, by comparing the R parameter of the EIM with the MF parameter of the sEMG, it is shown that the decline laws of the two have strong consistency, so it is feasible and reasonable to use EIM as an evaluation index of muscle fatigue.

EIM provides a novel method for muscle fatigue evaluation from bioelectricity phenomenon and contraction mechanics. This technology can solve the problem of sEMG and other evaluation methods, since it has potential for long-term clinical application. However, this article only discusses the changes in the R parameters of the arm muscles. In the future, it is necessary to study the changes in reactance and phase during the fatigue process. At the same time, these laws can be used to study muscle fatigue in other muscles in the human body, such as in the legs and abdomen.

REFERENCES

[1] J. Wan, Z. Qin, P.-Y. Wang, Y. Sun, and X. Liu, "Muscle fatigue: General understanding and treatment," *Exp. Mol. Med.*, vol. 49, no. 10, 2017, Art. no. e384.

[2] E. P. Debold, R. H. Fitts, C. W. Sundberg, and T. M. Nosek, "Muscle fatigue from the perspective of a single crossbridge," *Med. Sci. Sports Exerc.*, vol. 48, no. 11, pp. 2270–2280, Nov. 2016.

[3] F. Oueslati, J. Boone, and S. Ahmaidi, "Respiratory muscle endurance, oxygen saturation index in vastus lateralis and performance during heavy exercise," *Respiratory Physiol. Neurobiol.*, vol. 227, pp. 41–47, Jun. 2016.

[4] L. H. Ferreira, A. C. Smolarek, P. D. Chilibeck, M. P. Barros, S. R. Mcanulty, B. J. Schoenfeld, B. A. Zandona, and T. P. Souza-Junior, "High doses of sodium bicarbonate increase lactate levels and delay exhaustion in a cycling performance test," *Nutrition*, vol. 60, pp. 94–99, Apr. 2019.

[5] S. Qiu, X. Zhao, R. Xu, L. Xu, J. Xu, F. He, H. Qi, L. Zhang, B. Wan, and D. Ming, "Ultrasound image analysis on muscle texture of vastus intermedius and rectus femoris under neuromuscular electrical stimulation," *J. Med. Imag. Health Inf.*, vol. 5, no. 2, pp. 342–349, Apr. 2015.

[6] S. Huang, S. Cai, G. Li, Y. Chen, K. Ma, and L. Xie, "SEMG-based detection of compensation caused by fatigue during rehabilitation therapy: A pilot study," *IEEE Access*, vol. 7, pp. 127055–127065, 2019.

[7] M. Cifrek, V. Medved, S. Tonković, and S. Ostojić, "Surface EMG based muscle fatigue evaluation in biomechanics," *Clin. Biomechanics*, vol. 24, no. 4, pp. 327–340, May 2009.

[8] M. Zhu, "Evaluation of surface electromyography based on signal characteristic change on exercise muscle fatigue," *Investigación Clínica*, vol. 60, no. 6, 2019.

[9] M. Patel, N. Makaram, S. Balasubramanian, and S. Ramakrishnan, "Analysis of muscle fatigue using electromyography signals in gastrocnemius muscle during isometric plantar flexion," *Int. J. Biosci., Biochem. Bioinf.*, vol. 8, no. 2, pp. 100–106, Feb. 2018.
[10] A. Greco, G. Valenza, A. Bicchi, M. Bianchi, and E. P. Scilingo, "Assessment of muscle fatigue during isometric contraction using autonomic nervous system correlates," *Biomed. Signal Process. Control*, vol. 51, pp. 42–49, May 2019.
[11] J. Shi, Y. Zheng, and Z. Yan, "The relationship between SEMG and change in pennation angle of brachialis," in *Proc. 29th Annu. Int. Conf. IEEE Eng. Med. Biol. Soc.*, Aug. 2007, pp. 4802–4805.
[12] A. Liu, Z. J. Wang, and Y. Hu, "Network modeling and analysis of lumbar muscle surface EMG signals during flexion–extension in individuals with and without low back pain," *J. Electromyography Kinesiol.*, vol. 21, no. 6, pp. 913–921, Dec. 2011.
[13] S. B. Rutkove, "Electrical impedance myography: Background, current state, and future directions," *Muscle Nerve*, vol. 40, no. 6, pp. 936–946, Dec. 2009.
[14] B. Sanchez and S. B. Rutkove, "Electrical impedance myography and its applications in neuromuscular disorders," *Neurotherapeutics*, vol. 14, no. 1, pp. 107–118, Jan. 2017.
[15] A. Venhorst, D. P. Micklewright, and T. D. Noakes, "The psychophysiological regulation of pacing behaviour and performance fatigability during long-distance running with locomotor muscle fatigue and exercise-induced muscle damage in highly trained runners," *Sports Med.-Open*, vol. 4, no. 1, p. 29, 2018.
[16] L. L. Wang, M. Ahad, A. Mcewan, J. Li, M. Jafarpoor, and S. B. Rutkove, "Assessment of alterations in the electrical impedance of muscle after experimental nerve injury via finite-element analysis," *IEEE Trans. Biomed. Eng.*, vol. 58, no. 6, pp. 1585–1591, Jun. 2011.
[17] L. Li, A. A. Stampas, H. Shin, X. Li, and P. Zhou, "Alterations in localized electrical impedance myography of biceps brachii muscles paralyzed by spinal cord injury," *Frontiers Neurol.*, vol. 8, pp. 253–261, Jun. 2017.
[18] M. Jafarpoor, J. Li, J. K. White, and S. B. Rutkove, "Optimizing electrode configuration for electrical impedance measurements of muscle via the finite element method," *IEEE Trans. Biomed. Eng.*, vol. 60, no. 5, pp. 1446–1452, May 2013.
[19] T. Orth, "Impedance changes in biceps brachii due to isometric contractions and muscle fatigue using electrical impedance myography (EIM)," Electronic Theses and Dissertations, 2013.
[20] L. Li, H. Shin, X. Li, S. Li, and P. Zhou, "Localized electrical impedance myography of the biceps brachii muscle during different levels of isometric contraction and fatigue," *Sensors*, vol. 16, no. 4, p. 581, Apr. 2016.
[21] S. Hang Pun, Y. Ming Gao, P. Mak, M. I. Vai, and M. Du, "Quasi-static modeling of human limb for intra-body communications with experiments," *IEEE Trans. Inf. Technol. Biomed.*, vol. 15, no. 6, pp. 870–876, Nov. 2011.
[22] Y. M. Gao, S. H. Pun, P. U. Mak, M. Du, and M. I. Vai, "A multilayer cylindrical volume conductor model for galvanic coupling intra-body communication," in *Proc. 7th Int. Conf. Inf., Commun. Signal Process. (ICICS)*, Dec. 2009.
[23] Y. M. Gao, H. Zhang, and S. Lin, "Electrical exposure analysis of galvanic-coupled intra-body communication based on the empirical arm models," *Biomed. Eng. Online*, vol. 17, no. 1, p. 71, 2018.
[24] X. Zeng, Y. Gao, S. Pan, B. Mai, M. Wei, and M. Du, "Effects of muscle conductivity on signal transmission of intra-body communications," *J. Electron. Meas. Instrum.*, vol. 27, no. 1, pp. 21–25, Nov. 2013.
[25] S. Gabriel, R. W. Lau, and C. Gabriel, "The dielectric properties of biological tissues: III. Parametric models for the dielectric spectrum of tissues," *Phys. Med. Biol.*, vol. 41, no. 11, pp. 2271–2293, Nov. 1996.
[26] R. Plonsey and D. B. Heppner, "Considerations of quasi-stationarity in electrophysiological systems," *Bull. Math. Biophys.*, vol. 29, no. 4, pp. 657–664, Dec. 1967.
[27] Y.-M. Gao, Z.-M. Wu, S.-H. Pun, P.-U. Mak, M.-I. Vai, and M. Du, "A novel field-circuit FEM modeling and channel gain estimation for galvanic coupling real IBC measurements," *Sensors*, vol. 16, no. 4, p. 471, Apr. 2016.
[28] Y. M. Gao, Y. T. Ye, and S. Lin, "Investigation of implantable signal transmission characteristics based on visible data of the human leg," *BioMed. Eng. OnLine*, vol. 16, no. 88, pp. 1–14, 2017.
[29] G. J. Esper, C. A. Shiffman, R. Aaron, K. S. Lee, and S. B. Rutkove, "Assessing neuromuscular disease with multifrequency electrical impedance myography," *Muscle Nerve*, vol. 34, no. 5, pp. 595–602, Nov. 2006.
[30] S. B. Rutkove, P. M. Fogerson, L. P. Garmirian, and A. W. Tarulli, "Reference values for 50-kHZ electrical impedance myography," *Muscle Nerve*, vol. 38, no. 3, pp. 1128–1132, Sep. 2008.
[31] C. A. Shiffman, R. Aaron, V. Amoss, J. Therrien, and K. Coomler, "Resistivity and phase in localized BIA," *Phys. Med. Biol.*, vol. 44, no. 10, pp. 2409–2429, Oct. 1999.
[32] S. B. Rutkove, R. Aaron, and C. A. Shiffman, "Localized bioimpedance analysis in the evaluation of neuromuscular disease," *Muscle Nerve*, vol. 25, no. 3, pp. 390–397, Mar. 2002.
[33] H. Gai, J. Wang, and Q. Tian, "Modified Debye model parameters of metals applicable for broadband calculations," *Appl. Opt.*, vol. 46, no. 12, p. 2229, Apr. 2007.
[34] S. Thongpanja, A. Phinyomark, C. Limsakul, and P. Phukpattaranont, "Application of mean and median frequency methods for identification of human joint angles using EMG signal," in *Information Science and Applications*. Berlin, Germany: Springer, 2015, pp. 689–696.
[35] M. A. Callejon, J. Reina-Tosina, D. Naranjo-Hernandez, and L. M. Roa, "Galvanic coupling transmission in intrabody communication: A finite element approach," *IEEE Trans. Biomed. Eng.*, vol. 61, no. 3, pp. 775–783, Mar. 2014.
[36] M. A. Callejon, P. Del Campo, J. Reina-Tosina, and L. M. Roa, "A parametric computational analysis into galvanic coupling intrabody communication," *IEEE J. Biomed. Health Inform.*, vol. 22, no. 4, pp. 1087–1096, Jul. 2018.
[37] P. W. Humphreys and A. R. Lind, "The blood flow through active and inactive muscles of the forearm during sustained hand-grip contractions," *The J. Physiol.*, vol. 166, no. 1, pp. 120–135, Apr. 1963.
[38] S. Baidya and M. A. Ahad, "Assessment of optimized electrode configuration for electrical impedance myography using genetic algorithm via finite element model," *J. Med. Eng.*, vol. 2016, pp. 1–7, Sep. 2016.

L. K. HUANG received the B.S. degree from the College of Electronic Information and Electrical Engineering, Fujian University of Technology, Fuzhou, China, in 2017. He is currently pursuing the M.S. degree with the College of Physical and Information Engineering, Fuzhou University. His current research interests include neural networks and biomedical signal detecting technology.

L. N. HUANG received the B.S. degree with the College of Optoelectronics and Information Engineering from Fujian Normal University, Fuzhou, China, in 2018. She is currently pursuing the M.S. degree with the College of Physical and Information Engineering, Fuzhou University. Her current research interests include intra-body communication and biomedical signal detecting technology.

Y. M. GAO received the Ph.D. degree in electrical engineering from Fuzhou University, Fuzhou, China, in 2010. He is currently a Professor with the College of Physical and Information Engineering, Fuzhou University. Since 2004, he has been involved in research in the areas of bioelectromagnetism and biomedical signal detecting technology.

Ž. LUČEV VASIĆ received the Dipl.Ing. and Ph.D. degrees in electrical engineering from the University of Zagreb, Zagreb, Croatia, in 2007 and 2014, respectively. She is currently an Assistant Professor with the Department of Electronic Systems and Information Processing, Faculty of Electrical Engineering and Computing, University of Zagreb. Her research activities are in the field of biomedical electronic instrumentation and human-body signal transmission. She is also a member of IFMBE and CROMBES. She serves as the Vice-President of the IEEE EMB Croatian Section.

M. CIFREK received the Dipl.Ing., M.Sc., and Ph.D. degrees in electrical engineering from the Faculty of Electrical Engineering and Computing, University of Zagreb, Zagreb, Croatia, in 1987, 1992, and 1997, respectively, all in electrical engineering. He is currently a Professor of electrical engineering with the Department of Electronic Systems and Information Processing, Faculty of Electrical Engineering and Computing, University of Zagreb. His research interests are focused on the design of biomedical instrumentation, and biomedical signal analysis for research and clinical applications. He is also a member of IFMBE, CROMBES, KoREMA, and HMD. Since 2005, he has been a member of the Croatian Academy of Engineering.

M. DU received the Ph.D. degree in electrical engineering from Fuzhou University, Fuzhou, China, in 2005. Since 2007, she has been the Associate Director of the Key Laboratory of Eco-Industrial Green Technology of Fujian Province, Nanping, China. She is currently a Professor and a Ph.D. Supervisor with Fuzhou University. Her research interests include smart instrument and photoelectric.